Geophys. J. Int. (1989) **98**, 213–222

The response of two joined quarter spaces to *SH* line sources located at the material discontinuity interface

Yehuda Ben-Zion
Department of Geological Sciences, University of Southern California, Los Angeles, CA 90089-0740, USA

Accepted 1989 January 12. Received 1988 December 27; in original form 1988 May 9

SUMMARY

Exact analytical solutions to problems of *SH* line force and line dislocation operating at the interface between two quarter spaces are derived and discussed. It is shown that the resulting fields differ from that of a homogeneous half space in the distribution of travel times, wave amplitudes and polarity of first motions. These effects are documented in the literature. It is, therefore, suggested that when constructing theoretical seismic displacement fields from source, path and site effects, it is important to use response functions that account for material heterogeneity in the source region. An extension of the formulation used in the case of *SH* line dislocation leads to a 3-D representation theorem which gives the displacement field in terms of the displacement discontinuities along the rupture area. The resulting overall size scaling parameter is the 'potency', which does not suffer from an ambiguity associated with seismic moment in the case of heterogeneous source region.

Key words: quarter spaces, heterogeneous source region, representation theorem

1 INTRODUCTION

Although most earthquakes originate along faults that separate different rock bodies, theoretical models of seismic rupture usually simplify the source region by assuming that slip takes place along a surface that is situated in a homogeneous region. The purpose of this paper is to study some consequences of allowing material discontinuity to exist in the source region. In Sections 2 and 3 we derive analytical expressions for *SH*-waves excited by line sources operating at the interface between two quarter spaces of different elastic moduli. We find that the resulting *SH* displacement fields differ in travel times, wave amplitudes and polarity of first motions from the fields in a homogeneous half space. We suggest that when interpreting observed seismic waves it is important to consider effects arising from material heterogeneity in the source region. Similar recommendations regarding the analysis of static deformation fields are given by Rybicki & Kasahara (1977), Mahrer & Nur (1979), Mahrer (1981) and others.

The paper is also concerned with formulation and conceptual problems that arise when the source region contains material discontinuity. Woodhouse (1981) indicated that the seismic moment tensor is indeterminant in such cases, as significantly different moment tensors can be obtained depending upon which side of the material discontinuity the source is assumed to lie. Heaton & Heaton (1989) recently demonstrated the same ambiguity in the moment of static dislocation occurring between different elastic materials. They concluded that seismic moment is not a satisfactory measure of the size of an earthquake. Instead, they suggested the use of the unambiguous parameter potency, defined by Ben-Menahem & Singh (1981, equation 4.94) as the integral of the slip over the rupture surface.

The ambiguity of the source location (on which side of the material discontinuity does it lie?) naturally suggests a study in which sources are located at the interface itself. In Section 2 of this paper the source is an impulse *SH* line force operating at the interface between two different quarter spaces. The medium response to the line force is used in Section 3 where a seismic source is modelled as a line *SH* dislocation at the material discontinuity. The resulting displacement field is scaled by the slip function alone. In Section 4 the formulation of the third section is abstracted to a form of a 3-D representation theorem in which the size scaling parameter is the potency. We suggest that such representation is a clear and simple vehicle for synthesizing the seismic fields that are radiated from realistic heterogeneous source regions.

2 *SH* LINE FORCE OPERATING AT THE INTERFACE BETWEEN TWO WELDED QUARTER SPACES

Consider the infinite strike slip fault model (shown in Fig. 1) consisting of two welded elastic quarter spaces. The left quarter space is called medium 1 and the right one medium 2. The rigidity and shear wave velocity of medium i, $i = 1$, 2, are denoted, respectively, by μ_i and β_i. A line impulse force operating on medium 2 at an infinitesimal distance,

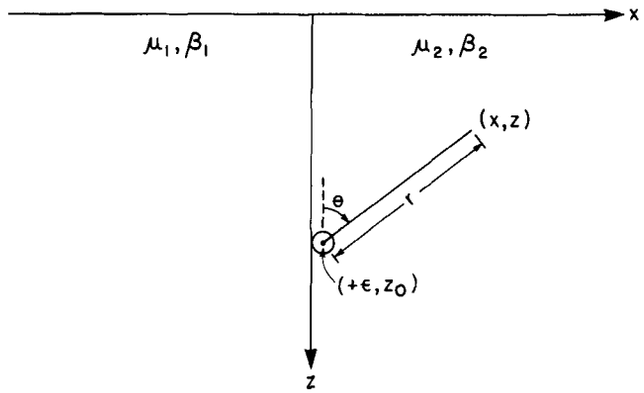

Figure 1. Two quarter spaces with *SH* line force operating on the quarter space $x > 0$ at horizontal source coordinate $\varepsilon \to 0$.

ε, from the interface is given by

$$\mathbf{F}_2 = [0, \mu_2\delta(t)\delta(x-\varepsilon)\delta(z-z_0), 0], \tag{1.1}$$

with $\delta(\ )$ denoting the Dirac delta function. This source is purely *SH* or antiplane and the displacement field everywhere is completely specified by $\mathbf{u}(\mathbf{x}, t) = [0, V(x, z, t), 0]$.

In this and the following section we obtain exact analytical solutions in time and space using the Cagniard–de Hoop method (Cagniard 1939, 1962; de Hoop 1960). An excellent explanation of the method can be found in chapter 6 of Aki & Richards (1980). In this method we first transform and solve wave equations in Laplace–Fourier domain. Second, we apply inverse Fourier transforms and find Laplace-space solutions in integral form. Finally we invert to the time–space domain by manipulating the Laplace-space integrals to look like forward Laplace transforms, from which the time–space solutions are immediately available as the expression in the integrands that multiply the Laplace operator e^{-st}.

The response of medium 2 to the source (1.1), denoted by V_{2S}, is governed by the inhomogeneous wave equation

$$\frac{1}{\beta_2^2}\frac{\partial^2 V_{2S}}{\partial t^2} - \left(\frac{\partial^2}{\partial x^2} + \frac{\partial^2}{\partial z^2}\right)V_{2S} = \delta(t)\,\delta(x-\varepsilon)\,\delta(z-z_0). \tag{1.2}$$

We transform (1.2) to Laplace–Fourier domain by operating on it with

$$\int_0^\infty e^{-st}\,dt \int_{-\infty}^{\infty} e^{-ik_x x}\,dx \int_{-\infty}^{\infty} e^{-ik_z z}\,dz,$$

we then get for the source wave

$$V_{2S}(k_x, k_z, s) = \frac{e^{-i(k_x\varepsilon + k_z z_0)}}{(s^2/\beta_2^2 + k_x^2 + k_z^2)}. \tag{1.3}$$

Applying one inverse Fourier transform to (1.3) we find

$$V_{2S}(x, k_z, s) = 1/2\pi \int_{-\infty}^{\infty} \frac{e^{-ik_z z_0}}{(s^2/\beta_2^2 + k_x^2 + k_z^2)} e^{ik_x(x-\varepsilon)}\,dk_x \tag{1.4}$$

and solving (1.4), using the Residue theorem, we obtain

$$V_{2S}(x, k_z, s) = 1/2\,\frac{e^{-ik_z z_0}\,e^{-(s^2/\beta_2^2 + k_z^2)^{1/2}|x-\varepsilon|}}{(s^2/\beta_2^2 + k_z^2)^{1/2}}. \tag{1.5}$$

Operating the second inverse Fourier transform (and changing the dummy variable k_z to k) we find for the source wave

$$V_{2S}(x, z, s) = 1/4\pi \int_{-\infty}^{\infty} \frac{e^{-ikz_0}}{(s^2/\beta_2^2 + k^2)^{1/2}} \times e^{-(s^2/\beta_2^2 + k^2)^{1/2}|x-\varepsilon|}\,e^{ikz}\,dk. \tag{1.6}$$

We now change variables by setting $k \equiv isp$ and get

$$V_{2S}(x, z, s) = 1/4\pi \int_{-i\infty}^{i\infty} B_{2S}\,e^{-s(pz + \eta_2|x-\varepsilon|)}\,dp \tag{1.7}$$

with $B_{2S} = -i/\eta_2\,e^{spz_0}$ and $\eta_2 = (\beta_2^{-2} - p^2)^{1/2}$, $\mathrm{Re}(\eta_2) \geqslant 0$.

The interaction of the source wave (1.7) with the welded vertical interface at $x = 0$ results in a reflected wave in medium 2, V_{2R}, and a transmitted wave in medium 1, V_{1T}, given by

$$V_{2R} = 1/4\pi \int_{-i\infty}^{i\infty} B_{2R}\,e^{-s(pz + \eta_2 x)}\,dp$$
$$V_{1T} = 1/4\pi \int_{-i\infty}^{i\infty} B_{1T}\,e^{-s(pz - \eta_1 x)}\,dp, \tag{1.8}$$

where the coefficient functions B_{2R} and B_{1T}, found by imposing the continuity of stress and displacement across the interface $x = 0$, are

$$B_{2R} = \frac{I_2 - I_1}{I_2 + I_1} B_{2S}$$

and

$$B_{1T} = \frac{2I_2}{I_2 + I_1} B_{2S},$$

with $I_i = \mu_i\eta_i$, $i = 1, 2$ and $\eta_i = (\beta_i^{-2} - p^2)^{1/2}$, $\mathrm{Re}(\eta_i) \geqslant 0$.

So far the existence of a free surface in the medium was not considered. Thus the set (1.7), (1.8) corresponds to the case of two welded half spaces. We now specify the plane $z = 0$ to be a free surface. This implies that the stress must vanish on the surface $z = 0$, resulting in reflected waves back to the medium $z > 0$. We obtain the solution to this problem of two welded quarter spaces by simply adding to the field (1.7), (1.8) the response, denoted by V^i, of two welded half spaces to an image source located at $(\varepsilon, -z_0)$. Doing so and letting $\varepsilon \to 0$, the response of the two welded quarter spaces to the source (1.1) (in Laplace-space domain) is

Medium 1

$$V_1 = V_{1T} + V_{1T}^i = 1/4\pi \int_{-i\infty}^{i\infty} B_{1T}\,e^{-s(pz - \eta_1 x)}\,dp + 1/4\pi \int_{-i\infty}^{i\infty} B_{1T}\,e^{-s(-pz - \eta_1 x)}\,dp \tag{1.9}$$

Medium 2

$$\begin{aligned} V_2 &= V_{2S} + V_{2R} + V_{2S}^i + V_{2R}^i \\ &= 1/4\pi \int_{-i\infty}^{i\infty} B_{2S}\,e^{-s(pz + \eta_2 x)}\,dp \\ &\quad + 1/4\pi \int_{-i\infty}^{i\infty} B_{2R}\,e^{-s(pz + \eta_2 x)}\,dp \\ &\quad + 1/4\pi \int_{-i\infty}^{i\infty} B_{2S}\,e^{-s(-pz + \eta_2 x)}\,dp \\ &\quad + 1/4\pi \int_{-i\infty}^{i\infty} B_{2R}\,e^{-s(-pz + \eta_2 x)}\,dp, \end{aligned}$$

with B_{2S}, B_{1T}, B_{2R} and η_i given in (1.7) and (1.8).

We are now ready to perform the Cagniard–de Hoop inversion by transforming the terms in the set (1.9) to look like forward Laplace transforms. We demonstrate this process on the term V_{2R}. The remaining five terms are evaluated in similar fashion.

We begin the inversion of V_{2R} by noticing that the integrand in V_{2R} can be written as $E(p)+i0(p)$, where $E(p)$, $0(p)$ are even, odd functions of p, respectively. Since the range of integration in V_{2R} is symmetric in p we have

$$\int_{-i\infty}^{i\infty}(\ )\,dp = 2\int_0^{i\infty} E(p)\,dp = 2\int_0^{i\infty}\mathrm{Re}(\ )\,dp$$
$$= 2i\,\mathrm{Im}\int_0^{i\infty}(\ )\,dp$$

or explicitly

$$V_{2R}(x,z,s) = 1/2\pi \times \mathrm{Im}\int_0^{i\infty}\frac{I_2-I_1}{I_2+I_1}\frac{1}{\eta_2}\mathrm{e}^{-s[p(z-z_0)+\eta_2 x]}\,dp. \quad (1.10)$$

Since η_1, η_2 are multivalued functions, four Riemann sheets are needed in order for the integrand in (1.10) to be an analytic function. The physical sheet is the one on which $\mathrm{Re}(\eta_1)\geqslant 0$, $\mathrm{Re}(\eta_2)\geqslant 0$ so that the radiation condition is satisfied. The sheets are connected along the four branch cuts given by $\mathrm{Re}(\eta_1)=0$, $\mathrm{Re}(\eta_2)=0$.
We next set

$$p(z-z_0)+\eta_2 x \equiv t \quad (1.11)$$

and inverting (1.11) we obtain a parameterization of the variable p as

$$p_2^{\mp}(t) = \begin{pmatrix} \mp(\cos\theta/r)t \pm (\sin\theta/r)(r^2/\beta_2^2-t^2)^{1/2} & t<r/\beta_2 \\ \mp(\cos\theta/r)t + i(\sin\theta/r)(t^2-r^2/\beta_2^2)^{1/2} & t>r/\beta_2 \end{pmatrix}, \quad (1.12)$$

where $\theta=\tan^{-1}[x/|z-z_0|]$ (measured positive in the clockwise direction) and $r=[x^2+(z-z_0)^2]^{1/2}$ are the angle and distance, respectively, between the source and the observation point as shown in Fig. 1. In (1.12) we take $p_2^{\mp}(t)$ depending on whether $z\lesseqgtr z_0$. This choice of signs insures that the points $p_2^{\mp}(t)=0$ correspond to non-negative values of the time parameter t.

We now construct the Cagniard path in the complex p domain by letting t in (1.12) vary from x/β_2 to ∞. Fig. 2 shows the Riemann sheet $\mathrm{Re}(\eta_1)\geqslant 0$, $\mathrm{Re}(\eta_2)\geqslant 0$ for the case $\beta_1>\beta_2$ and $z_0>z$. Indicated in Fig. 2 are the integration range in (1.10), Cagniard paths, upper connecting arc with radius R and the branch cuts. Two possible Cagniard paths, C_1 and C_2 are shown. C_1 corresponds to the case $\theta<\theta_{c21}=\cos^{-1}(\beta_2/\beta_1)$ and C_2 to $\theta>\theta_{c21}$. Since the integrand in (1.10) is analytic in the regions between the positive imaginary axis and Cagniard paths, and as by Jordan's lemma it goes to zero on the upper connecting path when R tends to ∞, (1.10) can be substituted by

$$V_{2R}(x,z,s) = 1/2\pi\,\mathrm{Im}\int_{\substack{\text{Cagniard}\\ \text{path}}}\frac{I_2-I_1}{I_2+I_1}\frac{1}{\eta_2}\mathrm{e}^{-st}\frac{dp_2^{\mp}}{dt}\,dt$$
$$= 1/2\pi\,\mathrm{Im}\int_{t=x/\beta_2}^{\infty}\left(\frac{I_2-I_1}{I_2+I_1}\frac{1}{\eta_2}\frac{dp_2^{\mp}}{dt}\right)\mathrm{e}^{-st}\,dt, \quad (1.13)$$

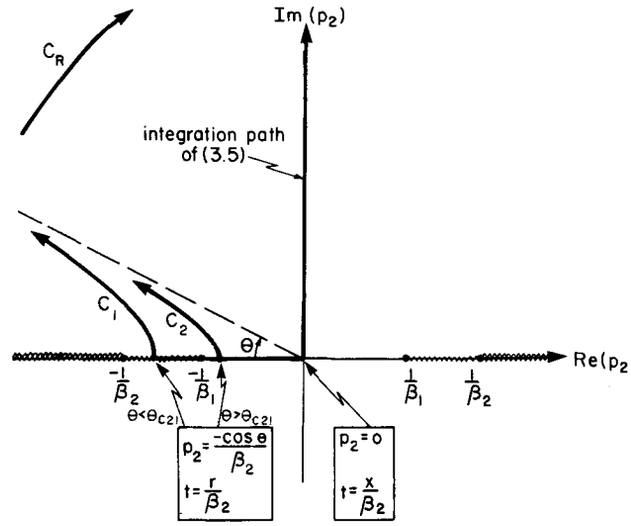

Figure 2. Schematic diagram of the Riemann sheet $\mathrm{Re}(\eta_1)\geqslant 0$, $\mathrm{Re}(\eta_2)\geqslant 0$, for the case $\beta_1>\beta_2$ and $z_0>z$. Heavy lines indicate the integration path of (1.10), two possible Cagniard paths (C_1 for $\theta<\theta_{c21}$ and C_2 for $\theta>\theta_{c21}$) and upper connecting path. Wiggly lines indicate the branch cuts $|\mathrm{Re}(p)|>1/\beta_1$, $|\mathrm{Re}(p)|>1/\beta_2$.

from which the time–space response can now be identified as

$$V_{2R}(x,z,t) = 1/2\pi\,\mathrm{Im}\left(\frac{I_2-I_1}{I_2+I_1}\frac{1}{\eta_2}\frac{dp_2^{\mp}}{dt}\right)_{p_2^{\mp}(t)} h(t-x/\beta_2), \quad (1.14)$$

where $h(\ )$ is the Heaviside unit step function and $dp_2^{\mp}/dt$ (with $\mp$ corresponding to $z\lesseqgtr z_0$) from (1.11) and (1.12) is given by

$$\frac{dp_2^{\mp}}{dt} = \begin{pmatrix} \mp\eta_2/(r^2/\beta_2^2-t^2)^{1/2} & t<r/\beta_2 \\ i\eta_2/(t^2-r^2/\beta_2^2)^{1/2} & t>r/\beta_2 \end{pmatrix}. \quad (1.15)$$

Now from (1.14), (1.12) and (1.15) it is clear that if $\beta_2>\beta_1$ then $p_2^{\mp}$, $dp_2^{\mp}/dt$ and the reflection coefficient $B_2(p_2^{\mp})=(I_2-I_1)/(I_2+I_1)$ are all real for $t<r/\beta_2$ and complex only for $t>r/\beta_2$, when the Cagniard path leaves the $\mathrm{Re}(p_2^{\mp})$ axis. Thus for $\beta_2>\beta_1$ the first motion corresponds to the arrival time of the regular geometrically reflected wave, traveling along the direct ray path from the source at the interface to the observation point with β_2 velocity. On the other hand, if $\beta_1>\beta_2$ (see Fig. 2) then the above situation holds only for $\theta>\theta_{c21}$ where $p_2^{\mp}$, $dp_2^{\mp}/dt$ and $B_2(p_2^{\mp})$ are still real for $t<r/\beta_2$. For $\theta<\theta_{c21}$, however, $B_2(p_2^{\mp})$ becomes complex for $|p_2^{\mp}|>|1/\beta_1|$ since then η_1 is pure imaginary and given by $\eta_1=-i\bar{\eta}_1$, $\bar{\eta}_1=(p_2^{\mp 2}-\beta_1^{-2})^{1/2}$. Here the time of the first arrival, t_{h2}, is found by setting $p_2^{\mp}=\mp 1/\beta_1$ in (1.11). This corresponds to the arrival of a head wave that travels from the source along the vertical interface with the faster β_1 velocity and then along a ray path with the critical angle to the observation point with β_2 velocity.

From the above considerations we now rewrite (1.14) in the more explicit form

$$V_{2R}(x,z,t) = 1/2\pi\,\mathrm{Re}\left(\frac{I_2-I_1}{I_2+I_1}\right)_{p_2^{\mp}} W_2 \quad h(t-r/\beta_2)$$
$$\mp h(\beta_1-\beta_2)h(\theta_{c21}-\theta)1/2\pi$$
$$\times\,\mathrm{Im}\left(\frac{I_2-I_1}{I_2+I_1}\right)_{p_2^{\mp}}\bar{W}_2$$
$$\times\,[h(t-t_{h2})-h(t-r/\beta_2)] \quad (1.16)$$

with $W_2 = (t^2 - r^2/\beta_2^2)^{-1/2}$, $\bar{W}_2 = (r^2/\beta_2^2 - t^2)^{-1/2}$, $t_{h2} = 1/\beta_1 |z_0 - z| + (\beta_2^{-2} - \beta_1^{-2})^{1/2} x$ and $\mp$ being determined by $z \lessgtr z_0$.

The remaining five waves (V_{1T}, V_{1T}^i, V_{2S}, V_{2S}^i and V_{2R}^i) are evaluated in similar ways. The final result for the time–space response of the two welded quarter spaces to the impulse *SH* line source is

Medium 1 ($x < 0$)

$$V_{1T}(x, z, t) = \mu_2/\pi \operatorname{Re}\left(\frac{\eta_1}{I_2 + I_1}\right)_{p_1^{\mp}} W_1 \quad h(t - r/\beta_1)$$
$$\pm h(\beta_2 - \beta_1) h(\theta_{c12} - \theta) \mu_2^2/\pi \left(\frac{\eta_1 \bar{\eta}_2}{\bar{I}_2^2 + I_1^2}\right)_{p_1^{\mp}}$$
$$\times \bar{W}_1 \quad [h(t - t_{h1}) - h(t - r/\beta_1)] \tag{1.17}$$
$$V_{1T}^i(x, z, t) = \mu_2/\pi \operatorname{Re}\left(\frac{\eta_1}{I_2 + I_1}\right)_{p_1^i} W_1^i \quad h(t - r_i/\beta_1)$$
$$+ h(\beta_2 - \beta_1) h(\theta_{c12} - \theta_i) \mu_2^2/\pi \left(\frac{\eta_1 \bar{\eta}_2}{\bar{I}_2^2 + I_1^2}\right)_{p_1^i}$$
$$\times \bar{W}_1^i \quad [h(t - t_{h1}^i) - h(t - r_i/\beta_1)]$$

and

$$V_1 = V_{1T} + V_{1T}^i.$$

Medium 2 ($x > 0$)

$$V_{2S}(x, z, t) = 1/2\pi\, W_2 \quad h(t - r/\beta_2)$$
$$V_{2S}^i(x, z, t) = 1/2\pi\, W_2^i \quad h(t - r_i/\beta_2)$$
$$V_{2R}(x, z, t) = 1/2\pi \operatorname{Re}\left(\frac{I_2 - I_1}{I_2 + I_1}\right)_{p_2^{\mp}} W_2 \quad h(t - r/\beta_2)$$
$$\pm h(\beta_1 - \beta_2) h(\theta_{c21} - \theta) \mu_1 \mu_2/\pi \left(\frac{\bar{\eta}_1 \eta_2}{I_2^2 + \bar{I}_1^2}\right)_{p_2^{\mp}}$$
$$\times \bar{W}_2 \quad [h(t - t_{h2}) - h(t - r/\beta_2)]$$
$$V_{2R}^i(x, z, t) = 1/2\pi \operatorname{Re}\left(\frac{I_2 - I_1}{I_2 + I_1}\right)_{p_2^i} W_2^i \quad h(t - r_i/\beta_2)$$
$$+ h(\beta_1 - \beta_2) h(\theta_{c21} - \theta_i) \mu_1 \mu_2/\pi \left(\frac{\bar{\eta}_1 \eta_2}{I_2^2 + \bar{I}_1^2}\right)_{p_2^i}$$
$$\times \bar{W}_2^i \quad [h(t - t_{h2}^i) - h(t - r_i/\beta_2)]$$

and

$$V_2 = V_{2S} + V_{2S}^i + V_{2R} + V_{2R}^i$$
$$= 1/2\pi \left[1 + \operatorname{Re}\left(\frac{I_2 - I_1}{I_2 + I_1}\right)_{p_2^{\mp}}\right] W_2 \quad h(t - r/\beta_2)$$
$$\pm h(\beta_1 - \beta_2) h(\theta_{c21} - \theta) \mu_1 \mu_2/\pi \left(\frac{\bar{\eta}_1 \eta_2}{I_2^2 + \bar{I}_1^2}\right)_{p_2^{\mp}}$$
$$\times \bar{W}_2 \quad [h(t - t_{h2}) - h(t - r/\beta_2)]$$
$$+ 1/2\pi \left[1 + \operatorname{Re}\left(\frac{I_2 - I_1}{I_2 + I_1}\right)_{p_2^i}\right] W_2^i \quad h(t - r_i/\beta_2)$$
$$+ h(\beta_1 - \beta_2) h(\theta_{c21} - \theta_i) \mu_1 \mu_2/\pi \left(\frac{\bar{\eta}_1 \eta_2}{I_2^2 + \bar{I}_1^2}\right)_{p_2^i}$$
$$\times \bar{W}_2^i \quad [h(t - t_{h2}^i) - h(t - r_i/\beta_2)]$$

where

$$\eta_j = (\beta_j^{-2} - p^2)^{1/2}, \qquad \bar{\eta}_j = (p^2 - \beta_j^{-2})^{1/2}, \; I_j = \mu_j \eta_j, \; \bar{I}_j = \mu_j \bar{\eta}_j,$$
$$W_j = (t^2 - r^2/\beta_j^2)^{-1/2}, \qquad \bar{W}_j = (r^2/\beta_j^2 - t^2)^{-1/2} \text{ for } j = 1,2$$
$$\theta = \tan^{-1}[x/|z_0 - z|], \qquad r = [x^2 + (z_0 - z)^2]^{1/2}$$
$$\theta_{c12} = \cos^{-1}(\beta_1/\beta_2), \qquad \theta_{c21} = \cos^{-1}(\beta_2/\beta_1)$$
$$t_{h1} = 1/\beta_2 |z_0 - z| + (\beta_1^{-2} - \beta_2^{-2})^{1/2} |x|,$$
$$t_{h2} = 1/\beta_1 |z_0 - z| + (\beta_2^{-2} - \beta_1^{-2})^{1/2} x,$$
$$p_1^{\mp} = \begin{bmatrix} \mp(\cos\theta/r)t \mp (\sin\theta/r)(r^2/\beta_1^2 - t^2)^{1/2} & t < r/\beta_1 \\ \mp(\cos\theta/r)t - i(\sin\theta/r)(t^2 - r^2/\beta_1^2)^{1/2} & t > r/\beta_1 \end{bmatrix}$$
$$p_2^{\mp} = \begin{bmatrix} \mp(\cos\theta/r)t \pm (\sin\theta/r)(r^2/\beta_2^2 - t^2)^{1/2} & t < r/\beta_2 \\ \mp(\cos\theta/r)t + i(\sin\theta/r)(t^2 - r^2/\beta_2^2)^{1/2} & t > r/\beta_2 \end{bmatrix},$$

θ_i, r_i, t_{h1}^i and t_{h2}^i are given from θ, r, t_{h1} and t_{h2}, respectively, by the substitution $z \to -z$, and p_1^i and p_2^i, W_j^i and $\bar{W}_j^i$ are given, respectively, from p_1^-, p_2^-, W_j and $\bar{W}_j$ by the substitutions $\theta \to \theta_i$ and $r \to r_i$.

From the set (1.17) it is seen that all the waves become infinite in amplitude immediately after the geometrical arrivals (direct for the source wave and regular reflections/transmissions for the rest). In addition, the terms that contain head wave contribution also become infinite in amplitude immediately before the geometrical arrivals, thus containing two singularities. These singularities are, however, integrable. They result from the discontinuous action of our idealized source and disappear when we synthesize the response due to a more realistic source by convolving the realistic source time function with the set (1.17).

Figure 3 shows schematically various ray paths of the different first arrivals in the set (1.17) for the case $\beta_1 > \beta_2$, $z_0 > z$. In the faster medium 1 there are two such arrivals at each observation point. The first corresponds to the wave transmitted through the vertical interface and the second to the transmitted wave that is also reflected by the free surface. The slower medium 2 on the other hand is divided into three distinct zones. In the first zone $0 < \theta < \theta_{c21}$ there are four different arrivals. The first corresponds to the head wave, the second to the simultaneous arrival of the source

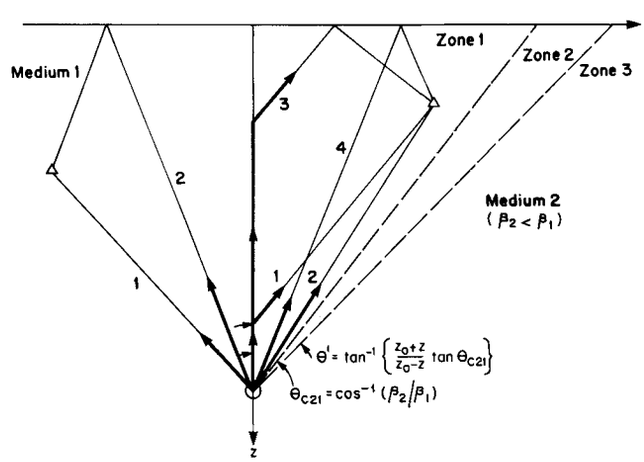

Figure 3. Various ray paths in the two quarter spaces for the case $\beta_1 > \beta_2$, $z_0 > z$.

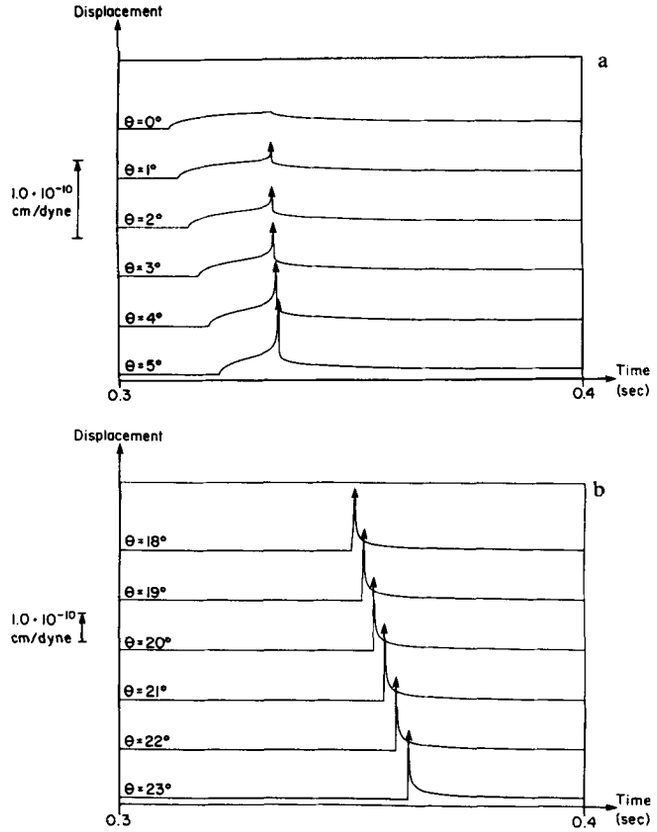

Figure 4. (a) V_2 of (1.17) for $z_0 = 1$ km, $z = 0$, $\theta = 0$, 1, 2, 3, 4 and 5°, $\beta_1 = 3.213$ km s^{-1}, $\mu_1 = 0.276 \times 10^{12}$ dyne cm^{-2}, $\beta_2 = 3.0$ km s^{-1} and $\mu_2 = 0.225 \times 10^{12}$ dyne cm^{-2}. (b) V_2 of (1.17) for $\theta = 18$, 19, 20, 21, 22 and 23°. The other parameters are the same as in (a).

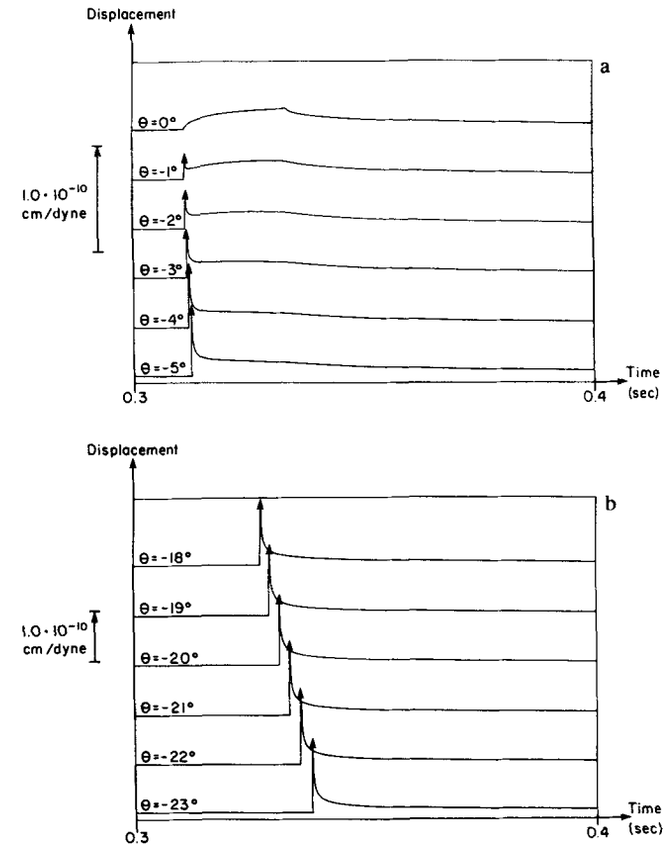

Figure 5. (a) V_1 of (1.17) for same parameters as in Fig. 4(a). (b) V_1 of (1.17) for same parameters as in Fig. 4(b).

wave and the wave reflected from the vertical interface, the third to the head wave that is reflected by the free surface and the fourth to the source wave and the reflected wave from the vertical interface that are also reflected by the free surface. The second zone $\theta_{c2l} < \theta < \theta' = \tan^{-1}[(z_0 + z)/(z_0 - z)\tan\theta_{c2l}]$ is characterized by $\theta > \theta_{c2l}$, $\theta_i < \theta_{c2l}$. Here there are three different arrivals of the second, third and fourth types of the zone $\theta < \theta_{c2l}$. In the third zone $\theta > \theta'$ both θ and $\theta_i > \theta_{c2l}$ and the situation is similar to the one of medium 1 in that there are only two different arrivals being the second and fourth types of the zone $\theta < \theta_{c2l}$.

Figure 4(a) shows the displacement field V_2 of (1.17) for source and observation parameters $z_0 = 1$ km, $z = 0$ and $\theta = 0$, 1, 2, 3, 4 and 5°. The medium parameters are $\beta_1 = 3.213$ km s^{-1}, $\mu_1 = 0.276 \times 10^{12}$ dyne cm^{-2}, $\beta_2 = 3.0$ km s^{-1} and $\mu_2 = 0.225 \times 10^{12}$ dyne cm^{-2}. The moderate contrast between the parameters of the different quarter spaces is well within the range of values found by laboratory measurements (Carmichael 1982) and field velocity studies of the San Andreas fault in central California (McEvilly 1966; Stewart 1968; Boore & Hill 1973; Walter & Mooney 1982). Fig. 4(b) shows the same as Fig. 4(a) for $\theta = 18$, 19, 20, 21, 22 and 23°. The solutions were calculated for time points separated by 10^{-4} s and linear interpolation was used in plotting the results. The critical angle is $\theta_{c2l} \simeq 20.9°$. For $\theta < \theta_{c2l}$ the first motion is due to a head wave arriving at $t = t_{h2}$. Gradual buildup of the head wave amplitude produces an emergent pulse which precedes the sharp singularity that arrives at $t = r/\beta_2$. The time range $r/\beta_2 - t_{h2}$ is decreasing to zero as θ approaches the critical angle and no head wave exists for $\theta > \theta_{c2l}$. Figs. 5(a) and (b) show the displacement field V_1 for the same parameters as in Fig. 4(a) and (b), respectively. Close to the interface $x = 0$ the continuity boundary conditions distort the shape of the $1/\sqrt{}$ decay curve that follows the singularity at $t = r/\beta_1$. This effect is rapidly diminishing as the angle θ increases. For the sake of comparison, Fig. 6 shows corresponding displacement fields in a homogeneous half space characterized by

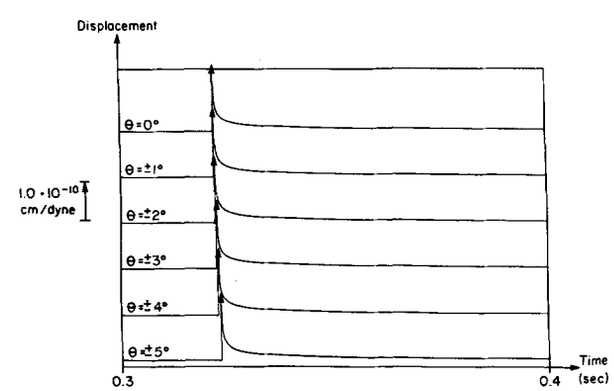

Figure 6. V_1 and V_2 in homogeneous half space characterized by $\mu = (\mu_1 + \mu_2)/2 = 0.2505 \times 10^{12}$ dyne cm^{-2} and $\beta = (\beta_1 + \beta_2)/2 = 3.1065$ km s^{-1} for $\theta = 0$, ±1, ±2, ±3, ±4 and ±5°. The other parameters are the same as in Fig. 4(a).

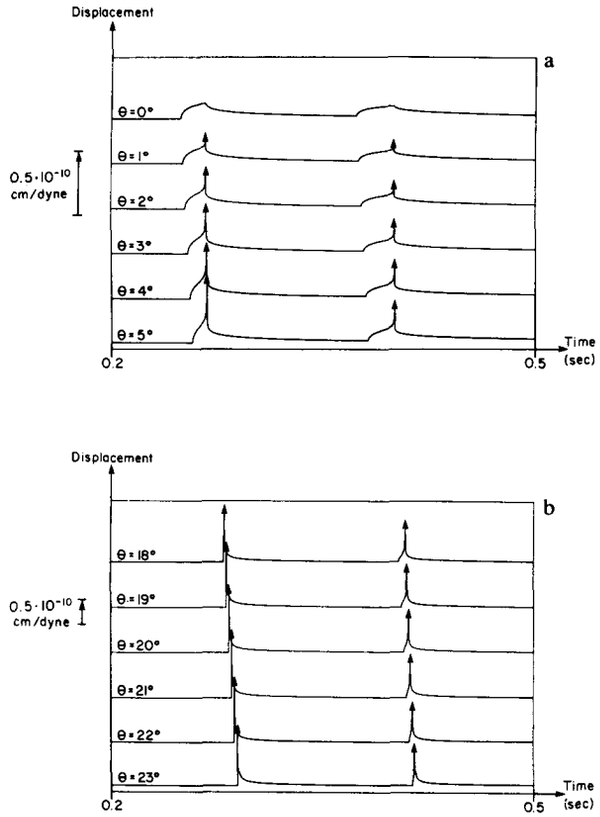

Figure 7. (a) V_2 of (1.17) for $z = 200$ m. The other parameters are the same as in Fig. 4(a). (b) V_2 of (1.17) for $z = 200$ m. The other parameters are the same as in Fig. 4(b).

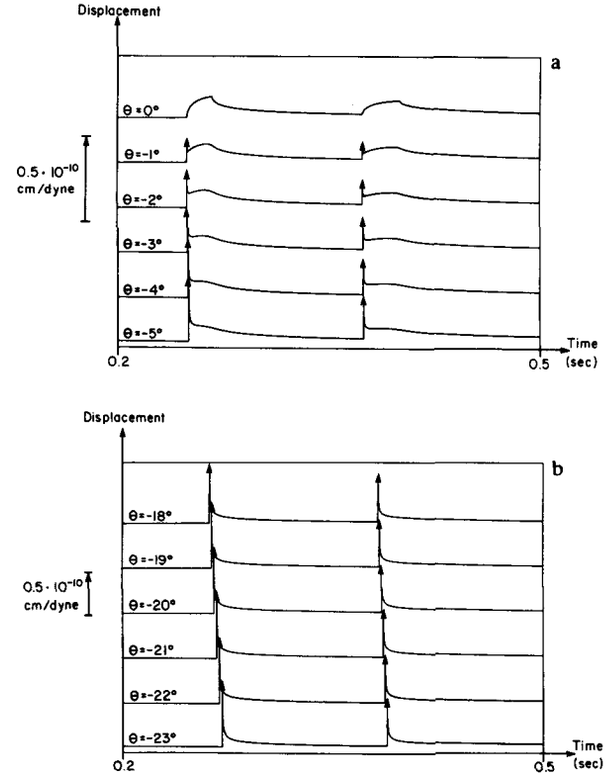

Figure 8. (a) V_1 of (1.17) for same parameters as in Fig. 7(a). (b) V_1 of (1.17) for same parameters as in Fig. 7(b).

the average values $\mu = (\mu_1 + \mu_2)/2 = 0.2505 \times 10^{12}$ dyne cm^{-2} and $\beta = (\beta_1 + \beta_2)/2 = 3.1065$ km s^{-1}, for $\theta = 0$, ± 1, ± 2, ± 3, ± 4 and $\pm 5°$. A glance across Figs 4(a), 5(a) and 6 immediately shows that the material discontinuity results in prominent features which cannot be accounted for in the framework of a homogeneous half space model. A more detailed discussion on the differences between the displacement fields in our model of heterogeneous source region and the corresponding ones in a model of homogeneous half space are given in the next section and in the discussion part of the paper. Figs 7(a) and (b) show V_2 for an observation depth $z = 200$ m and the other parameters the same as in 4(a) and (b), respectively. Here $\theta' = 29.9°$. For $\theta < \theta_{c21} < \theta'$ the four different arrivals of Fig. 3 are clearly shown. For $\theta_{c21} < \theta < \theta'$ it is seen that the reflected waves from the free surface still contain head wave contributions. Finally, Figs. 8(a) and (b) show V_1 for the same parameters as in 7(a) and (b), respectively. Figs 4–8 clearly show that the displacement fields in media 1 and 2 are significantly different from each other and from the corresponding fields of a homogeneous half space.

The problem we considered in this section may correspond to man made experiments where unbalanced (external) force systems are operating on the medium and the resulted displacement fields are continuous everywhere. In the next section we model the displacement field due to the internal phenomenon of spontaneous rupture.

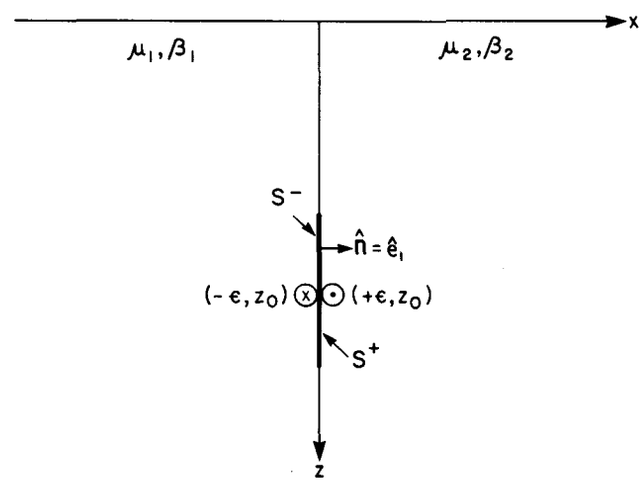

Figure 9. Two quarter spaces with *SH* line dislocation operating at the interface between the different media. The heavy line represents a fault surface S across which displacement discontinuities may occur. $\mathbf{n}$ is the normal to S pointing from S^- to S^+.

3. *SH* LINE DISLOCATION AT THE INTERFACE BETWEEN TWO QUARTER SPACES

In this section we calculate the response of two quarter spaces to spontaneous introduction at the interface $x = 0$ of *SH* dislocation (Fig. 9) specified by

$$\Delta V(0, z, t) = |\Delta V|\, \delta(z - z_0) h(t). \tag{2.1}$$

Here the system is self balanced since the total force and

torque due to a dislocation source are zero (Aki & Richards 1980, chapter 3).

In the case of two half spaces, the radiated wave field in Laplace-space domains (see 1.8) is

$$V_1 = 1/4\pi \int_{-i\infty}^{i\infty} B_1 \, e^{-s(pz-\eta_1 x)} \, dp \qquad x<0$$
$$V_2 = 1/4\pi \int_{-i\infty}^{i\infty} B_2 \, e^{-s(pz+\eta_2 x)} \, dp \qquad x>0. \tag{2.2}$$

Transforming (2.1) to Laplace-space domain, and putting it in a form that is compatible with V_1 and V_2 of (2.2), we get

$$\Delta V(0, z, s) = 1/4\pi \int_{-i\infty}^{i\infty} -2i\,|\Delta V|\, e^{-sp(z-z_0)} \, dp$$
$$= 1/4\pi \int_{-i\infty}^{i\infty} B_S \, e^{-spz} \, dp, \tag{2.3}$$

where here

$$B_S = -2i\,|\Delta V|\, e^{spz_0}.$$

Now the displacement boundary condition at the interface $x=0$ is given by

$$(V_2 - V_1)_{x=0} = \Delta V \tag{2.4a}$$

and the stress boundary condition at $x=0$ by

$$\mu_1(\partial V_1/\partial x)_{x=0} = \mu_2(\partial V_2/\partial x)_{x=0}. \tag{2.4b}$$

Solving (2.4a) and (2.4b) using (2.2) and (2.3) we find

$$B_1 = [-I_2/(I_1+I_2)]B_S \quad \text{and} \quad B_2 = [I_1/(I_1+I_2)]B_S.$$

From here the time-space solutions for V_1 and V_2 are immediately available by simple substitutions from V_{1T} and V_{2R} of (1.17). Adding, as before, the response of two half spaces to an image source, the response of two quarter spaces to the slip (2.1) is found to be

Medium 1 ($x<0$)

$$V_1 + V_1^i = -\Delta V/\mu_1\pi \,\mathrm{Re}\left(\frac{I_1 I_2}{I_2+I_1}\right)_{p_1^{\mp}} W_1 \quad h(t-r/\beta_1)$$
$$\pm h(\beta_2-\beta_1)h(\theta_{c12}-\theta)\Delta V/\mu_1\pi\left(\frac{I_1^2\bar{I}_2}{I_1^2+\bar{I}_2^2}\right)_{p_1^{\mp}}$$
$$\times \bar{W}_1 \quad [h(t-t_{h1}) - h(t-r/\beta_1)]$$
$$-\Delta V/\mu_1\pi \,\mathrm{Re}\left(\frac{I_1 I_2}{I_2+I_1}\right)_{p_1^i} W_1^i \quad h(t-r_i/\beta_1)$$
$$+ h(\beta_2-\beta_1)h(\theta_{c12}-\theta_i)\Delta V/\mu_1\pi\left(\frac{I_1^2\bar{I}_2}{I_1^2+\bar{I}_2^2}\right)_{p_1^i}$$
$$\times \bar{W}_1^i \quad [h(t-t_{h1}^i) - h(t-r_i/\beta_1)] \tag{2.5}$$

Medium 2 ($x>0$)

$$V_2 + V_2^i = \Delta V/\mu_2\pi \,\mathrm{Re}\left(\frac{I_1 I_2}{I_1+I_2}\right)_{p_2^{\mp}} W_2 \quad h(t-r/\beta_2)$$
$$\mp h(\beta_1-\beta_2)h(\theta_{c21}-\theta)\Delta V/\mu_2\pi\left(\frac{I_2^2\bar{I}_1}{I_2^2+\bar{I}_1^2}\right)_{p_2^{\mp}}$$
$$\times \bar{W}_2 \quad [h(t-t_{h2}) - h(t-r/\beta_2)]$$
$$+ \Delta V/\mu_2\pi \,\mathrm{Re}\left(\frac{I_1 I_2}{I_1+I_2}\right)_{p_2^i} W_2^i \quad h(t-r_i/\beta_2)$$
$$- h(\beta_1-\beta_2)h(\theta_{c21}-\theta_i)\Delta V/\mu_2\pi\left(\frac{I_2^2\bar{I}_1}{I_2^2+\bar{I}_1^2}\right)_{p_2^i}$$
$$\times \bar{W}_2^i \quad [h(t-t_{h2}^i) - h(t-r_i/\beta_2)],$$

where all the definitions of (1.17) hold.

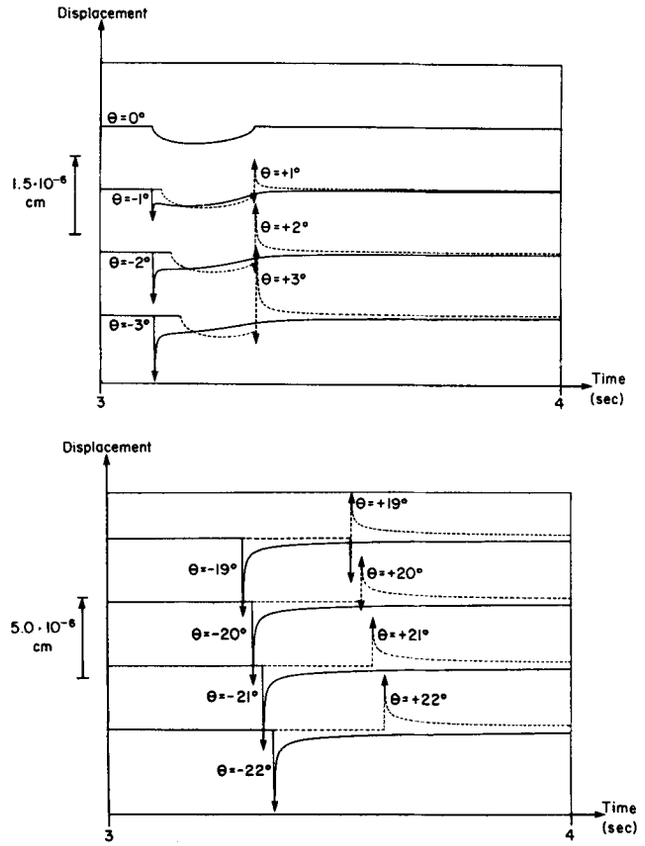

Figure 10. (a) V_1 (solid line) and V_2 (dashed line) of (2.5) for $z_0 = 10$ km, $\Delta V = 1$ cm, $z=0$ and $\theta = 0$, ± 1, ± 2 and $\pm 3°$. The media velocities and rigidities are the same as in Fig. 4(a). (b) Same as (a) for $\theta = \pm 19$, ± 20, ± 21 and $\pm 22°$.

Figure 10(a) shows V_1 (solid line) and V_2 (dashed line) of the field (2.5) for $z_0 = 10$ km, $\Delta V = 1$ cm, $z=0$ and $\theta = 0$, ± 1, ± 2 and $\pm 3°$. Fig. 10(b) shows the same for $\theta = \pm 19$, ± 20, ± 21 and $\pm 22°$. The media velocities and rigidities are the same as in Fig. 4(a). The solutions were calculated for time points separated by 10^{-3} s and linear interpolation was used in plotting the results. In the faster medium 1 all the displacement is in the negative y direction. The first motion at all angles occurs at $t = r/\beta_1$ with the arrival of the singularity $V_1 \to -\infty$ that is associated with the geometrical rays. Following that the displacement field decays along $1/\sqrt{}$ curve, with some distortion close to the interface $x=0$. In the slower medium 2, for $\theta < \theta_{c21}$ the first motion is in the negative y direction when the head wave arrives at $t = t_{h2}$. The amplitude of the wave increases gradually (with some distortion near the interface $x=0$) over the time range $r/\beta_2 - t_{h2}$ and V_2 approaches $-\infty$ just before the arrival of the geometrical rays at $t = r/\beta_2$. Immediately after $t = r/\beta_2$ V_2 comes back from $+\infty$, decaying from there along the $1/\sqrt{}$ curve. For $\theta > \theta_{c21}$ all the displacement V_2 is in the positive y direction, beginning with the arrival of the

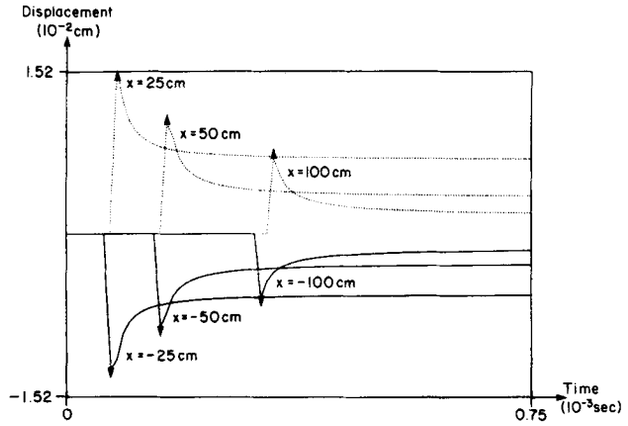

Figure 11. Same as Fig. 10(a) for $z = z_0 = 10$ km and $x = \pm 25$, ± 50 and ± 100 cm.

geometrical rays singularity $V_2 \to +\infty$ at $t = r/\beta_2$ and decaying from there along the $1/\sqrt{\ }$ curve.

An overall view of the wavefield brings out two places where the waveform undergoes radical changes. One is across the interface $x = 0$ separating the two different elastic materials and the other is across the critical angle. For observation depths below the free surface a third such location exists across the angle θ'.

Figure 11 demonstrates the field close to the dislocation by showing the early parts of V_1 and V_2 of (2.5) for $z = z_0 = 10$ km and $x = \pm 25$, ± 50 and ± 100 cm. The other parameters are the same as in Fig. 10(a). Here the solutions were calculated for time points separated by 10^{-5} s and linear interpolation was used in plotting the results. The existence of the displacement discontinuity in $(x_0, z_0) = (0, 10\,\text{km})$ is evident from the permanent components of displacements, with reversed polarity and increased magnitude toward the interface, in the fields V_1 and V_2.

Figure 12 shows the corresponding displacement field in the homogeneous half space model of Fig. 6, at $\theta = 0$, ± 1, ± 2 and $\pm 3°$. The other parameters are the same as in Fig. 10(a). A comparison between Figs 10(a) and 12 shows that when the two media on the opposite sides of the fault are taken to be dissimilar the three most commonly measured

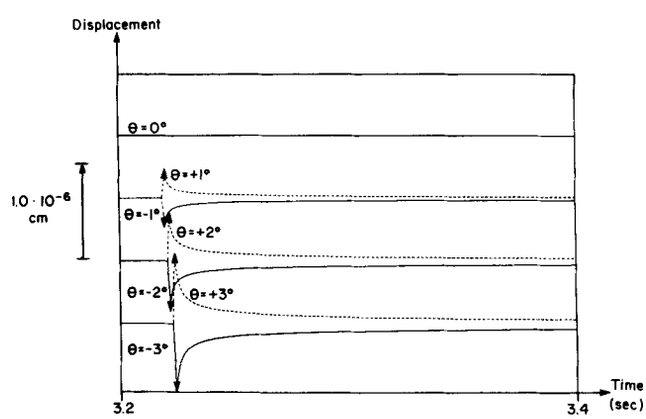

Figure 12. Same as Fig. 10(a) for the homogeneous half space model of Fig. 6.

features of seismograms, the distribution of travel times, wave amplitudes and polarity of first motions, are all different from what is expected in the framework of a homogeneous half space. For slip in a homogeneous medium the amplitudes and arrival times of first motion are symmetric through the epicentre. For a slip surface between dissimilar media, the amplitudes in the more compliant medium 2 are larger than in the stiffer medium 1 and the first arrivals in the slower medium are delayed with respect to the faster medium. Perhaps more important still, the polarity of first motion in the region $\theta < \theta_{c21}$ in the more compliant medium 2 is reversed from the polarity expected in a homogeneous medium. In the discussion part of the paper we bring references documenting these possible effects of material discontinuities across faults.

4. A 3-D REPRESENTATION THEOREM

In this part we generalize the formulation of the previous section to a 3-D representation theorem by which seismic waves are synthesized from the displacement discontinuities across the rupture surface.

Let $B_{ij}(\mathbf{x}, t; \xi, \tau, \mathbf{n})$ denote the ith component of displacement at observation coordinates and time $(\mathbf{x}, t)$ due to a unit point dislocation in the jth direction at source coordinates and time (ξ, τ), occurring across a surface S characterized at ξ by its unit normal vector $\mathbf{n}(\xi)$. (The letter B is used to prevent confusion between the response here to a unit dislocation and the usual Green tensor response to a unit force, for which the letter G is traditionally used.) The situation $\mathbf{e}_j \cdot \mathbf{n} = 0$, $\mathbf{e}_j$ being the unit vector in the jth direction, corresponds to a shear crack, while $\mathbf{e}_j \times \mathbf{n} = 0$, represents a tension crack. Let $\Delta u_j(\xi, \tau)$ be the jth component of the displacement discontinuity across S at (ξ, τ), i.e. $\Delta u_j(\xi, \tau) = u_j(\xi, \tau)|_{s^+} - u_j(\xi, \tau)|_{s^-}$ where s^+ and s^- denote the positive and negative sides of the rupture surface, respectively, as shown in Fig. 9. The u_i component of displacement at observation coordinates and time is then simply obtained by summing $\Delta u_j B_{ij}$ over the source coordinates and time, giving

$$u_i(\mathbf{x}, t) = \int_{-\infty}^{\infty} d\tau \iint_S \Delta u_j(\xi, \tau) B_{ij}(\mathbf{x}, t; \xi; \tau, \mathbf{n})\, ds, \tag{3.1}$$

where the convention of summing repeated indexes applies.

It is interesting to compare (3.1) with the elastodynamic representation theorem given by de Hoop (1958). When the only sources are displacement discontinuities de Hoop's theorem (Aki & Richards 1980, equation 3.2) gives

$$u_i(\mathbf{x}, t) = \int_{-\infty}^{\infty} d\tau \iint_S m_{jk} \partial G_{ij}(\mathbf{x}, t; \xi, \tau)/\partial \xi_k\, ds, \tag{3.2}$$

where $m_{jk} = \Delta u_p n_q C_{pqjk}$ is the seismic moment density tensor, C_{pqjk} is the tensor of elastic constants and G_{ij} denotes a Green tensor which satisfies displacement and stress continuity across the fault surface S. For shear faulting in an isotropic medium equation (3.2) can be written (Paul Richards, personal communication) as

$$u_i(\mathbf{x}, t) = \int_{-\infty}^{\infty} d\tau \iint_S \Delta u_j(\xi, \tau) n_k \{\mu[\partial G_{ij}(\mathbf{x}, t; \xi; \tau)/\partial \xi_k + \partial G_{ik}(\mathbf{x}, t; \xi, \tau)/\partial \xi_j]\}\, ds \tag{3.3}$$

and comparing (3.1) with (3.3) we see that for shear faulting in an isotropic medium

$$B_{ij}(\mathbf{x}, t; \xi, \tau, \mathbf{n}) = n_k \mu[\partial G_{ij}(\mathbf{x}, t; \xi, \tau)/\partial \xi_k + \partial G_{ik}(\mathbf{x}, t; \xi, \tau)/\partial \xi_j]. \quad (3.4)$$

In (3.2) and (3.3) the displacement field is generated by couples and force dipoles, operating along the fault surface with strength at each point on the fault proportional to the seismic moment density tensor at that point. When the seismic source is moved an infinitesimal distance across a material discontinuity interface the rigidity and the seismic moment jump in magnitude, however, the { } bracket of (3.3), being traction, is continuous across the material discontinuity interface and this tells us that these different seismic moments produce the same displacement field. This is, essentially, the argument of Woodhouse (1981) and Heaton & Heaton (1989), indicating the ambiguity of the seismic moment in cases of heterogeneous source region. The above argument shows that in such cases the seismic moment is not a good scaling parameter for the size of earthquakes (Heaton & Heaton 1989). In fact, μ can be cancelled internally in { } of (3.3) and in the right hand side of (3.4). This is easily understood when we remember that G_{ij} is the solution of an inhomogeneous wave equation. In the case of a shear wave, the multiplication of the source term by μ just cancels the division of the inhomogeneous term of the wave equation by the same factor (see 1.1 and 1.2). In the case of a compressional wave these two operations produce the dimensionless material constant $(1-2\nu)/(2-2\nu)$, ν being Poisson's ratio (Heaton & Heaton 1989). This cancelling appearance of material constants is not present in (3.1) and in the left hand side of (3.4) since the response function B_{ij} is constructed from a solution of a homogeneous wave equation. There, the material constants enter the solution only through the boundary conditions and not through a source term. Thus, for shear faulting, the displacement field in the representation (3.1) is synthesized directly from the unambiguously defined slip function and the resulting overall size scaling parameter is the potency, in accord with Ben-Menahem & Singh (1981) and Heaton & Heaton (1989).

We also note that the use of (3.1) requires B_{ij} to be known along the rupture surface only while G_{ij} of (3.2) is needed in a whole region containing the rupture area. Alternatively, $\partial G_{ij}/\partial \xi_k$ can be solved for directly along the rupture area. We bring up this point because when the medium is heterogeneous the Cagniard–de Hoop inversion for the full wave field can be performed only when the sources are located directly at the material discontinuity surface.

In light of the above considerations we suggest that, at least in the case of heterogeneous source region, (3.1) is easier to use and more natural to interpret than (3.2).

5. DISCUSSION

The sites of many earthquakes are on high offset geological faults which are surfaces of material discontinuity in the earth. Seismic field studies near the San Andreas fault in central California (McEvilly 1966; Stewart 1968; Boore & Hill 1973; Walter & Mooney 1982) indicate that the materials along the opposite sides of the fault are significantly different in their seismic properties. As summarized in Mooney & Ginzberg (1986), numerous other seismic studies (Healy & Peake 1975; Feng & McEvilly 1983; Cormier & Spudich 1984), gravity surveys (Pavoni 1973; Wang *et al.* 1978; Stierman 1984) and geological and physical considerations (Sibson 1977) suggest that in some cases heterogeneous fault zone structures extend throughout the entire crust.

Motivated by the above studies and the theoretical works of Woodhouse (1981) and Heaton & Heaton (1989) we studied simple 2-D *SH* cases in which sources are located at an interface separating two different elastic quarter spaces. We found that the resulting displacement fields differ from the corresponding fields of a homogeneous half space in the distribution of the three most commonly measured features of seismograms, travel times, wave amplitudes and polarity of first motions.

The possible effects of dissimilar media across a fault zone have been documented. Boore & Hill (1973) and Engdahl & Lee (1976) showed that when material heterogeneity across the San Andreas fault in central California is incorporated into hypocentre inversion, earthquakes which in a homogeneous model fall 2–3 km west of the fault, are relocated on the fault. Wallace, Helmberger & Ebel (1981) studying the Santa Barbara earthquake of August 13, 1978 pointed out an apparent asymmetry in the intensity of shaking, with regions northwest of the epicentre subject to more intense shaking. The magnitude of the earthquake determined by Caltech instruments located to the southeast was found to be $M_L = 5.1$ (Whitcomb & Hutton 1978) while the magnitude determined by northern California data was significantly larger, $M_L = 5.7$. These asymmetries may be the consequence of the material heterogeneity across the fault.

In a homogeneous medium the polarity of first motion is antisymmetric with respect to the fault. From Fig. 10(a) it is seen that when the medium is assumed heterogeneous, the polarity of the first motion for the region $\theta < \theta_{c21} = \arccos(\beta_2/\beta_1) \sim 21°$ in the slower medium 2, is reversed from what is anticipated in the homogeneous case. This is due to the fact that in this region the first motion is due to a head wave with polarity of first motion as the one of the faster medium on the opposite side of the fault. Wallace *et al.* (1981), using a homogeneous fault zone model, found that the fault plane solution inferred from the near field displacements is significantly different from that determined from the teleseismic data. They indicated that vertical structure similar to that of Fig. 1 can reconcile the near- and far-field inferred fault plane solutions.

There are several controversial large high frequency accelerations recorded in the near field of the 1979 Imperial Valley earthquake (Archuleta 1982; Spudich & Cranswick 1982; Hartzell & Heaton 1983) and the 1966 Parkfield earthquake (Aki 1968; Anderson 1974; Trifunac & Udwadia 1974; Lindh & Boore 1981). The 1966 Parkfield earthquake accelerogram of a near field station located 80 m from the fault also contains high frequency vibrations that precede the main pulse (Aki 1968). These phases may be interface waves (similar to the head wave of Fig. 10a) resulting from material discontinuity interfaces in the fault zone. Such phases can contribute significant amplitudes to the near-field waves.

In view of the effects that a typical material discontinuity has on the resulting displacement fields, illustrated in the present work for the *SH* 2-D case, existing theoretical solutions for homogeneous fault zone models may fail to account for important features of the waves radiated by earthquakes. This is especially important for near field or strong ground motion studies.

A representation theorem, equation (3.1), provides for a general 3-D displacement field in terms of the medium response to point dislocations and the displacement discontinuity function along the rupture area. The resulting overall size scaling parameter is the potency which does not suffer from the ambiguity associated, in the case of heterogeneous source region, with seismic moment.

A practical use of the representation (3.1) in modelling realistic sources requires the entire B_{ij} tensor, corresponding to point dislocations occurring, in general, in material discontinuity interface. The derivation of such a tensor will be taken up in a following work.

ACKNOWLEDGMENTS

I thank Keiiti Aki, Vincent Lee and Francisco Sánchez-Sesma for stimulating discussions. Constructive comments and suggestions by Bernard Minster, Paul Richards, Peter Leary, Egill Hauksson and Journal reviewers are gratefully acknowledged. Sue Turnbow and Desser Moton patiently typed the manuscript. Janet Dodds drafted the figures. The author was supported during this research by a W. M. Keck Foundation fellowship.

REFERENCES

Aki, K., 1968. Seismic displacement near a fault, *J. geophys. Res.*, **73**, 5359–5376.

Aki, K. & Richards, P. G., 1980. *Quantitative Seismology Theory and Methods, Vol.* 1, W. H. Freeman, San Francisco.

Andersen, J., 1974. A dislocation model for the Parkfield Earthquake, *Bull. seism. Soc. Am.*, **64**, 671–686.

Archuleta, R. J., 1982. Analysis of near-source static and dynamic measurements from the 1979 Imperial Valley earthquake, *Bull. seism. Soc. Am.*, **72**, 1927–1956.

Ben-Menahem, A. & Singh, S. J., 1981. *Seismic Waves and Sources*, Springer-Verlag, New York.

Boore, D. M. & Hill, D. P., 1973. Wave Propagation Characteristics in the Vicinity of the San Andreas fault, in Proc. Conf. Tectonic Problems of the San Andreas Fault System, *Stanford Univ. Pub., Geol. Sci.*, **13**, 215–224.

Cagniard, L., 1939. *Reflexion et Refraction es Ondes Seismiques Progressives*, Gauthier-Villars, Paris.

Cagniard, L., 1962. *Reflection and Refraction of Progressive Seismic Waves*, translated and revised by Flinn, E. A. & Dix, C. H., McGraw-Hill, New york.

Carmichael, R. S., 1982. *Handbook of Physical Properties of Rocks, Vol. II*, CRC Press, Boca Raton, Fl.

Cormier, V. F. & Spudich, P., 1984. Amplification of ground motion and waveform complexity in fault zones: examples from the San Andreas and Calaveras faults, *Geophys. J. R. astr. Soc.*, **79**, 135–152.

de Hoop, A. T., 1958. Representation theorems for the displacement in an elastic solid and their application to elastodynamic diffraction theory, *thesis*, Technische Hogeschool Delft.

de Hoop, A. T., 1960. A modification of Cagniard's method for solving seismic pulse problems, *Appl. Sci. Res.*, **B8**, 349–356.

Engdahl, E. R. and Lee, W. H. K., 1976. Relocation of local earthquakes by seismic ray tracing, *J. geophys. Res.*, **81**, 4400–4406.

Feng, R. and McEvilly, T. V., 1983. Interpretation of seismic reflection profiling data for the structure of the San Andreas fault zone, *Bull. seism. soc. Am.*, **73**, 1701–1720.

Hartzell, S. H. & Heaton, T. H., 1983. Inversion of strong motion and teleseismic waveform data for the fault rupture history of the 1979 Imperial Valley, California, earthquake, *Bull. seism. Soc. Am.*, **73**, 1553–1583.

Healy, J. H. & Peake, L. G., 1975. Seismic velocity structure along a section of the San Andreas fault near Bear Valley, California, *Bull. seism. Soc. Am.*, **65**, 1177–1197.

Heaton, H. T. & Heaton, R. E., 1989. Static deformations from point forces and force couples located in welded elastic Poissonian half-spaces: implications for seismic moment tensors, *Bull. seism. Soc. Am.*, 1989.

Lindh, A. G. & Boore, D. M., 1981. Control of rupture fault geometry during the 1966 Parkfield earthquake, *Bull. seism. Soc. Am.*, **71**, 95–116.

Mahrer, K. D. & Nur, A., 1979. Static strike–slip faulting in a horizontally varying crust, *Bull. seism. Soc. Am.*, **69**, 975–1009.

Mahrer, K. D., 1981. Strike–slip faulting in a bi-directionally varying crust, *Bull. seism. Soc. Am.*, **71**, 391–404.

McEvilly, T. V., 1966. Crustal structure estimation within a large scale array, *Geophys. J.*, **11**, 13–17.

Mooney, W. D. & Ginzburg, A., 1986. Seismic measurements of the internal properties of fault zones, *PAGEOPH*, **124**, 141–157.

Pavoni, N., 1973. A structural model for the San Andreas fault zone along the northeast side of the Gabilan range, in Proc. Conf. Tectonic Problems of the San Andreas Fault System, *Stanford Univ. Publ. Geol. Sci.*, **13**, 259–267.

Rybicki, K. & Kasahara, K., 1977. A strike–slip fault in a laterally inhomogeneous medium, *Tectonophysics*, **42**, 127–138.

Sibson, R. H., 1977. Fault rocks and fault mechanism, *J. geol. Soc. Lond.*, **133**, 191–213.

Stewart, S. W., 1968. Preliminary comparison of seismic traveltimes and inferred crustal structure adjacent to the San Andreas fault in the Diablo and Gabilan ranges of Central California, in Proc. Conf. Geological Problems of San Andreas Fault System, *Stanford Univ. Pub., Geol. Sci.*, **11**, 218–230.

Stierman, D. J., 1984. Geophysical and geological evidence for fracturing, water circulation, and chemical alteration in granitic rocks adjacent to major strike–slip faults, *J. geophys. Res.*, **89**, 5849–5857.

Spudich, P. & Cranswick, E., 1982. Use of near-source seismic-array data to reveal details of the earthquake rupture process, *Earthquake Notes*, **53**, 39.

Trifunac, M. D. & Udwadia, F. E., 1974. Parkfield, California earthquake of June 27, 1966: a three-dimensional moving dislocation, *Bull. seism. Soc. Am.*, **64**, 511–534.

Wallace, T. C., Helmberger, D. V. & Ebel, J. E., 1981. A broadband study of the 13 August 1978 Santa Barbara earthquake, *Bull. seism. Soc. Am.*, **71**, 1701–1718.

Walter, A. W. & Mooney, W. D., 1982. Crustal structure at the Diablo and Gabilan ranges, Central California: a reinterpretation of existing data, *Bull. seism. Soc. Am.*, **72**, 1567–1590.

Wang, C. Y., Lin, W. N. & Wu, F. T., 1978. Constitution of the San Andreas fault zone at depth, *Geophys. Res. Lett.*, **5**, 741–744.

Whitcomb, J. H. & L. K Hutton, 1978. On the magnitude of the August 13, 1978 Santa Barbara, California earthquake, *Trans. Am. geophys. Union*, **59**, 1130.

Woodhouse, J. H., 1981. The excitation of long period seismic waves by a source spanning a structural discontinuity, *Geophys. Res. Lett.*, **8**, 1129–1131.